Spectrochimica Acta Part A: Molecular and Biomolecular Spectroscopy 284 (2023) 121799

Contents lists available at ScienceDirect

Spectrochimica Acta Part A: Molecular and Biomolecular Spectroscopy

journal homepage: www.journals.elsevier.com/spectrochimica-acta-part-a-molecular-and-biomolecular-spectroscopy

A benzothiophene-quinoline-based targetable fluorescent chemosensor for detection of viscosity and mitochondrial imaging in live cells

Siqi Zhang [a,1], Hong Zhang [b,1], Lihe Zhao [a], Lanlan Xu [a], Pinyi Ma [a,*], Ping Ren [b,*], Daqian Song [a,*]

[a] College of Chemistry, Jilin Province Research Center for Engineering and Technology of Spectral Analytical Instruments, Jilin University, Qianjin Street 2699, Changchun 130012, China

[b] Department of Thoracic Surgery, The First Hospital of Jilin University, Changchun, Jilin, China

HIGHLIGHTS

- BQL demonstrated a large Stokes shift (minimizing interference from autofluorescence) and a good response to viscosity (using the TICT principle).
- BQL demonstrated little to no pH-dependency, polarity-dependency, or interference from other analytes.
- BQL was used to monitor viscosity changes in mitochondria induced by ion carriers, and was used to report on viscosity in real time during mitophagy.

GRAPHICAL ABSTRACT

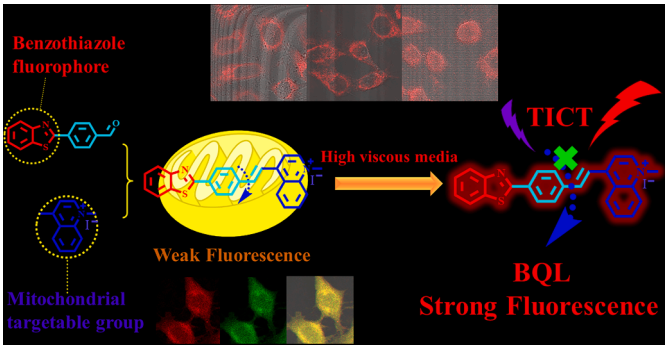

ARTICLE INFO

Keywords:
Fluorescent chemosensor
Viscosity
Mitochondrial imaging
Mitochondrial autophagy

ABSTRACT

Mitochondria are the sites of respiration in cells, and they participate in many indispensable biological processes. Because variations in mitochondrial viscosity can lead to dysfunctions of mitochondrial structure and function (and even induce malignant diseases), new sensors that can accurately monitor changes in mitochondrial viscosity are essential. To better investigate these changes, we report the development and evaluation of a novel benzothiophene-quinoline-based fluorescent chemosensor (BQL) that was designed especially for monitoring mitochondrial viscosity. BQL demonstrated a large Stokes shift (minimizing interference from autofluorescence) and a good response to viscosity (using the TICT principle). Moreover, BQL demonstrated little to no pH-dependency, polarity-dependency, or interference from other analytes. Thus, BQL has an excellent specificity for viscosity. BQL was used to monitor viscosity changes in mitochondria induced by ion carriers, and was used to report on viscosity in real time during mitophagy. To sum up, BQL provided a new approach for detecting viscosity in living cells and *in vivo*. BQL should prove to be an excellent tool for the analysis of viscosity changes in live cells.

* Corresponding authors.
E-mail addresses: mapinyi@jlu.edu.cn (P. Ma), rpemail@jlu.edu.cn (P. Ren), songdq@jlu.edu.cn (D. Song).

[1] These authors contributed equally to this work.

https://doi.org/10.1016/j.saa.2022.121799
Received 20 April 2022; Received in revised form 23 August 2022; Accepted 25 August 2022
Available online 2 September 2022

1. Introduction

Intracellular viscosity is an important index affecting the normal health and status of cells, influencing fundamental processes such as the diffusion of intracellular substances, common intracellular macromolecular interactions, signal transmission, and other vital biological processes[1–4]. By modulating these fundamental processes, intracellular viscosity can profoundly affect cell proliferation, cell differentiation, and cell apoptosis. Moreover, because changes in intracellular viscosity can affect these important cell processes, abnormal changes in viscosity can result in disease, including atherosclerosis[5], hypertension[6], malignancy[7], and Alzheimer's disease[8,9]. To monitor these potentially important changes in cellular viscosity, viscosity measurements in specific organelles are essential, especially because viscosity is known to inherently vary from region to region in the cell [10–14].

Mitochondria regulate nutrients to produce the energy they need to function effectively inside cells. As important 'power plants' in cells, mitochondria play an essential role in metabolism, respiration, differentiation, and aging[15–17]. Mitochondria also play important roles in the synthesis of biomacromolecules and the regulation of intracellular homeostasis[18]. Because abnormalities in the mitochondrial microenvironment can cause mitochondrial dysfunctions that are associated with neurological diseases, observations of mitochondrial viscosity are essential[19–21]. Thus far, numerous mitochondrial dyes have been designed to report on the mitochondrial microenvironment, and several can be used for rapid and sensitive detection[12,22–24]. In general, mitochondrial dyes are positively charged, and these are attracted into the mitochondria because of the negative mitochondrial potential. In recent years, fluorescence confocal imaging has become a popular and widespread method for investigating biological phenomenon, largely because its fast imaging speed, high signal intensity, and its ability to link *in vitro* and *in vivo* experiments[25–27]. Thus, fluorescence confocal imaging of mitochondrial viscosity holds great potential for monitoring physiological relevant events.

In this work, we have designed a novel fluorescent chemosensor (BQL) comprised of benzothiazole group, which functions as both a fluorescence emitter and an electron-donating group, and a quinoline derivative cation, which functions as both an electron-withdrawing group and a mitochondria-specific targeting group. In addition, we incorporated a benzene ring in the middle to expand the conjugated structure. Together, these functional groups form a D-π-A structure for viscosity detection. Generally, when a molecular rotor is combined with a fluorophore, the molecular rotor can rotate (relative to the whole molecule) in low viscosity solvent, allowing the relaxation process to proceed by non-radiative transition, and resulting in significant quenching of fluorescence. In contrast, non-radiative energy transitions are inhibited in high viscosity solvents, resulting in an enhancement of fluorescence intensity — the twisted intramolecular charge transfer (TICT) principle[28–30]. Through similar changes in its fluorescence, BQL may sensitively reflect viscosity changes associated with mitochondria-related physiological processes. With good spatiotemporal resolution and low cytotoxicity, BQL could potentially find wide application in medicine, biology, chemistry, and many other fields. Scheme 1 illustrates the sensing mechanism between BQL and viscosity.

2. Experimental section

2.1. Materials and instruments

Details of the materials and instruments used in this study can be found in the Supplementary information section.

2.2. Synthesis of BQL

The BQL synthetic process is described in Fig. 1.

Compound 1. 2-Bromobenzothiazole (214 mg, 1 mmol) and 4-formylphenylboronic acid (165 mg, 1.1 mmol) were dissolved in 17.5 mL of solvent (4:2:1 ratio of toluene, ethanol, and 2 mol/L sodium bicarbonate aqueous solution) in a three-necked flask with stirring. Next, tetrakis (triphenylphosphine) palladium (11.58 mg, 10 μmol) was added as a catalyst. Using freeze–thaw and a vacuum device, water vapor and oxygen were then removed from the flask. Next, the synthesis reaction was allowed to proceed at 78℃. After 9 h reaction, the product was extracted with dichloromethane and water. The lower organic phase was then dried with magnesium sulfate and filtered with a suction filter. The resulting liquid was rotary evaporated and then purified by column chromatographic separation. The final product (Compound 3) was eluted in dichloromethane/ absolute methanol (50:1). Finally, a yellowish solid was obtained (126.69 mg, 53 %). ^{1}H NMR (400 MHz, DMSO) δ 10.10 (s, 1H), 8.28 (d, 2H), 8.14 (dd, 1H), 7.98 (m, 3H), 7.56 (ddd, 1H), 7.45 (ddd, 1H) (Figure S1).

Compound 2. 4-Methyl quinoline and iodomethane were used to synthesize compound 2 [31,32].

BQL. Compound 1 (66.1 mg, 0.418 mmol) and compound 2 (100 mg, 0.418 mmol) were added to a dry flask and dissolved in 25 mL ethanol. Next, piperidine (165.5 μL) was added to the above mixture. The reaction was then refluxed with stirring at 80 °C for 10 h. The product was purified by TLC using dichloromethane/ absolute methanol (30:1). Finally, a deep yellow solid (BQL) was collected (42.79 mg, 27 %). ^{1}H NMR (400 MHz, DMSO-d_6) δ 9.43 (d, 1H), 9.12 (d, 1H), 8.56 (t, 1H), 8.54 – 8.47 (m, 2H), 8.34 – 8.29 (m, 1H), 8.26 (t, 3H), 8.21 (d, 3H), 8.11 (t, 2H), 7.60 (t, 1H), 7.52 (t, 1H), 4.59 (s, 3H) (Figure S2). MS (ESI): Calcd for $[C_{25}H_{19}N_2S]^+$: 379.13, found: 379.07 (Figure S3).

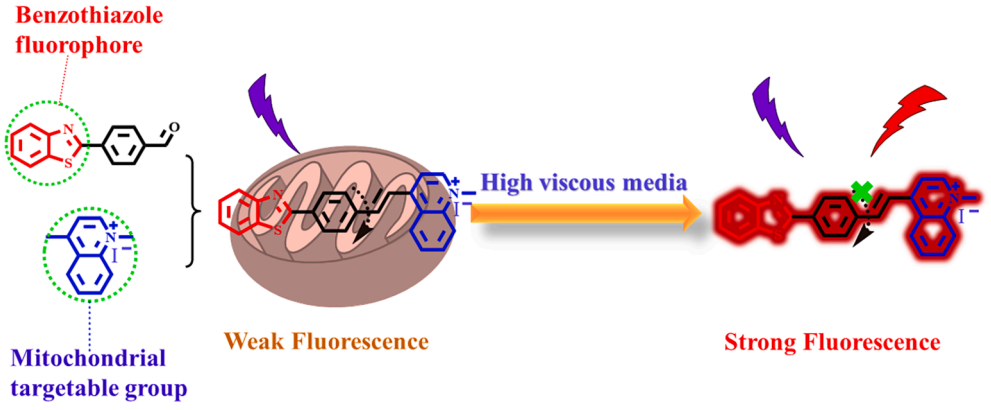

Scheme 1. The mechanism of BQL response to viscosity.

2.3. Preparation and measurement of samples

2.3.1. Sample treatment

The viscosity of the solvent was varied by adjusting the proportion of glycerol in a PBS-glycerol system (pH = 7.40, 10 mM PBS), and the resulting viscosity values were recorded using an NDJ-5S digital rotational viscometer. BQL stock solution (1 mM in ultrapure water) was stored in a −40 °C freezer protected from light. Each sample (10 μM) was prepared by dissolving 10 μL BQL in 990 μL of viscous solvent. All samples were ultrasonicated to remove air bubbles and maintained at 37 °C for 1 h. The fluorescence emission spectrum and UV–Vis absorption spectrum were then measured and recorded at 37 °C.

2.3.2. pH experiments

Starting from a PBS stock solution (pH = 7.40, 10 mM), we adjusted the pH of the solvent to 4.45, 5.49, 6.55, 7.40, 8.41, 9.89, and 10.66. These different pH solvents were used to explore the influence of pH on the chemosensor BQL. Each sample (10 μM) was prepared at the specified pH by adding 10 μL BQL stock solution to 990 μL of the relevant solvent.

2.3.3. Effects of common interfering analytes

To investigate the effects of common interfering substances on viscosity detection, we added Ca^{2+}, Cu^{2+}, Fe^{2+}, Fe^{3+}, K^{+}, Mg^{2+}, Mn^{2+}, Na^{+}, Pb^{2+}, Zn^{2+}, Cys, and GSH to PBS (pH = 7.40, 10 mM) to obtain solutions of the different interference analytes (final concentration, 50 μM). Sample solutions (10 μM) containing the specified common interfering substance were then prepared from these solutions. All solutions were maintained at 37 °C.

2.4. Cell experiments

2.4.1. Cytotoxicity assay

The MTT assay was used to evaluate the toxicity of BQL on A549 cells, and to find the optimum concentration conditions to conduct subsequent cell experiments. First, A549 cells were cultivated in a 96-well plate using a volume of 100 μL/well. Different concentrations of the BQL (from 10 to 100 μM) were then added to the A549 cells. Next, the cells were incubated for 24 h at 37 °C. MTT solution was then added into each well, and the cells were incubated for 4 h. The MTT solution was removed, and 150 μL of DMSO was added into each well. Finally, the cytotoxicity at each concentration was assessed using a microplate reader.

2.4.2. Co-localization experiments

A549 cells were incubated with the BQL (20 μM) for 5 min, and then with MitoTracker Green (20 nM) for 25 min. To explore target specificity, A549 cells were co-incubated with the BQL (5 μM) and LysoTracker (20 nM) for 25 min.

2.4.3. Viscosity measurements

First, mitochondrial viscosity was perturbed by addition of an ion carrier (monensin or nystatin). Monensin (final concentration, 6 μM) or nystatin (final concentration, 6 μM) was added to A549 cells, and the cells were then incubated for 25 min. Next, BQL (10 μM) was added, and the cells were incubated for an additional 20 min. The A549 cells were then washed three times with PBS and used for imaging.

Second, mitochondrial viscosity was perturbed by mitophagy. A549 cells were incubated with BQL (10 μM) in serum-free medium for 25 min or 60 min. A549 cells were then washed three times with PBS and used for imaging.

3. Results and discussion

3.1. Spectral response

The spectral response of BQL to viscosity was evaluated. In the absence of added glycerol (0 % glycerol), the viscosity of PBS was 0.70 cP. Glycerol was then added incrementally to PBS to prepare a set of viscous solvents with a viscosity gradient, reaching a maximum viscosity of 202.4 cP in 95 % glycerol. These viscous solvents were maintained at 37 °C for use in subsequent experiments. The fluorescence and UV–vis absorption spectrums of the different viscous solvents were subsequently measured at 37 °C. The UV–vis absorption spectrum of BQL obtained at the lowest and the highest viscosity (0.70 cP and 202.4 cP) revealed two UV–vis absorption peaks at 320 nm and 404 nm. These two peaks correspond to the benzothiazole fluorophore and quinoline derivative cation, respectively (Figure S4). The UV–vis absorption intensities of both peaks increased when the viscosity index increased.

A fluorescence spectrum series of the viscous solvents was also obtained. As the viscosity increases, the rotation ability of BQL at the rotating site is reduced. This is accompanied by a decrease in non-radiation transition in the BQL molecule after laser stimulation. According to the TICT principle, there should be a resultant enhancement in fluorescence intensity. BQL demonstrated the strongest fluorescence emission peak at 560 nm (Fig. 2A). The large Stokes shift had the advantages of low background interference, little photodamage to biological samples, strong sample penetration and high detection sensitivity. The observed Stokes shift was 128 nm, indicating that BQL has the additional advantage of anti-interference. Upon gradual addition of glycerol, the fluorescence intensity at 560 nm increased accordingly. The fluorescence intensity of BQL was observed to increase 14.3-fold over the full viscosity range. From the literature, mitochondrial viscosity is known to range from 1 cP to 100 cP, and the fluorescence intensity of BQL increased 9.3-fold in the mitochondrial viscous range.

To accomplish this, we investigated the mathematical relationship between viscosity values (within the range of mitochondrial viscosity) and their corresponding fluorescence intensities. As shown in Fig. 2B, the relationship between lg I_{560} and lg η could be fit to the Forster–Hoffmann equation ($\lg(I) = C + x \lg\eta$; R = 0.99624). The marked increase in fluorescence intensity observed indicates that BQL can be used as a tool for monitoring mitochondrial viscosity. As solvent viscosity increased, the quantum number of the emitted light also increased. This produced a notable change in the quantum yield (the ratio of the emitted quantum number to the absorbed quantum number), which increased from 0.21 % at the lowest viscosity to 1.26 % at the highest viscosity. The data related to the probe BQL were made into a clear table (Table S1).

3.2. Stability and selectivity

Because double bonds are known to decompose under laser

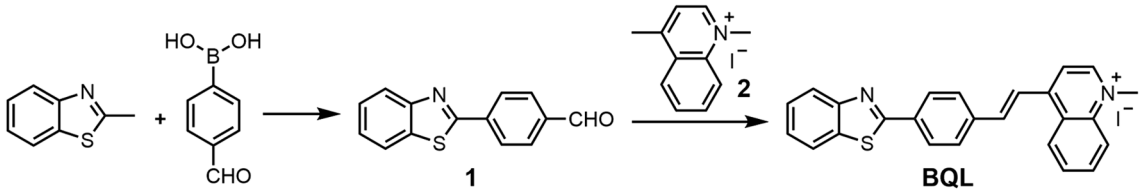

Fig. 1. The BQL synthetic process.

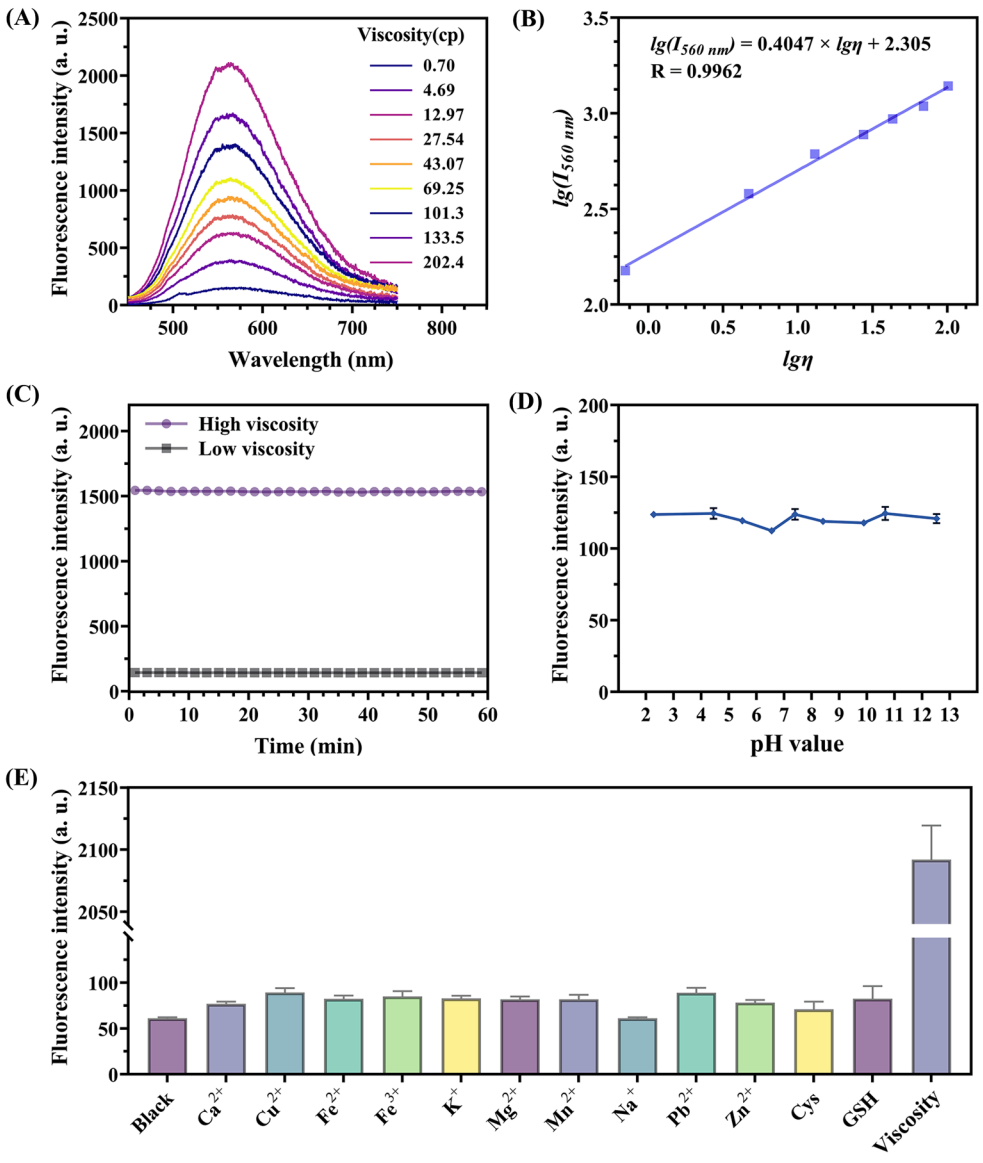

Fig. 2. (A) Fluorescence spectra of BQL following the gradual addition of glycerol to a PBS–glycerol system. (B) Fitting of the data to the Forster–Hoffmann equation showing the linear relationship between the fluorescence intensity (log I_{560}) and the viscosity (log η) of BQL, λ_{ex} = 432 nm. (C) Photostability of BQL (10 μM) under continuous irradiation by laser for 60 min in low viscosity and high viscosity conditions, λ_{ex} = 432 nm. (D) Fluorescence intensity response of BQL (10 μM) in PBS (with glycerol fixed) at different pH values, λ_{ex} = 432 nm. (E) Fluorescence response of BQL (10 μM) to 50 μM different analytes (Ca^{2+}, Cu^{2+}, Fe^{2+}, Fe^{3+}, K^{+}, Mg^{2+}, Mn^{2+}, Na^{+}, Pb^{2+}, Zn^{2+}, Cys, and GSH) (and viscous solvent for comparison), λ_{ex} = 432 nm.

illumination, we next tested the optical stability of the BQL chemosensor. The fluorescence intensity of BQL remained nearly unchanged after continuous excitation light irradiation for 60 min in low-viscous and high-viscous medium at 37℃ (Fig. 2C). Thus, the BQL chemosensor demonstrates excellent photostability. To investigate the response of BQL to pH, BQL fluorescence was recorded under different pH conditions. As shown in Fig. 2D, the fluorescence values did not fluctuate significantly in the pH 2.28 – 12.52 range, demonstrating that BQL had little to no interaction with hydroxide ions or hydrogen ions, and that the effects of pH on the BQL chemosensor could be ignored. Next, we performed polarity interference experiments in solvents of different polarities. As shown in Figure S5, the fluorescence intensity change of BQL in the most polarized solvent (DMSO) was markedly lower than that in viscous solvents. Thus, the effects of polarity on the chemosensor could also be ignored. Together, the above results indicate that BQL is a sensitive chemosensor with the capability for specific viscosity detection.

Finally, to investigate the specificity of the chemosensor, we performed experiments using potential interference analytes. As shown in Fig. 2E, the responses of BQL to common potential interfering species in cells (Ca^{2+}, Cu^{2+}, Fe^{2+}, Fe^{3+}, K^{+}, Mg^{2+}, Mn^{2+}, Na^{+}, Pb^{2+}, Zn^{2+}, Cys, and GSH) were negligible, even at high (50 μM) final concentrations. This could be attributed to the fact that the BQL molecular structure did not possess a reaction site for the interference analytes. In summary, BQL (with its benzothiazole group and a rotating site) could be applied to specifically identify mitochondrial viscosity in different complicated mediums without interference from other environmental factors.

3.3. Theoretical calculations

To better understand the inherent relationship between molecular rotation, solution viscosity, and fluorescence intensity, we performed theoretical calculations to explain the fluorescence phenomenon in detail. As shown in Fig. 3, in the ground state (S0), the structure of BQL was nearly planar. The HOMO was mainly located in the benzothiazolyl and phenyl groups, and the LUMO was located in the phenyl and methyl quinoline groups. Because both HOMO and LUMO were associated with the phenyl group, intramolecular charge transfer (ICT) was possible. Hence, BQL demonstrated strong fluorescence emission in its quasi-planar molecular structure. In the first excited state (S1), the benzothiazolyl and the methyl quinoline groups demonstrated a dihedral angle of about 90° (relative to each other) in the optimal BQL structure. As a consequence, the HOMO and the LUMO exhibited obvious charge separation with a TICT state. In agreement with electron hole theory, the

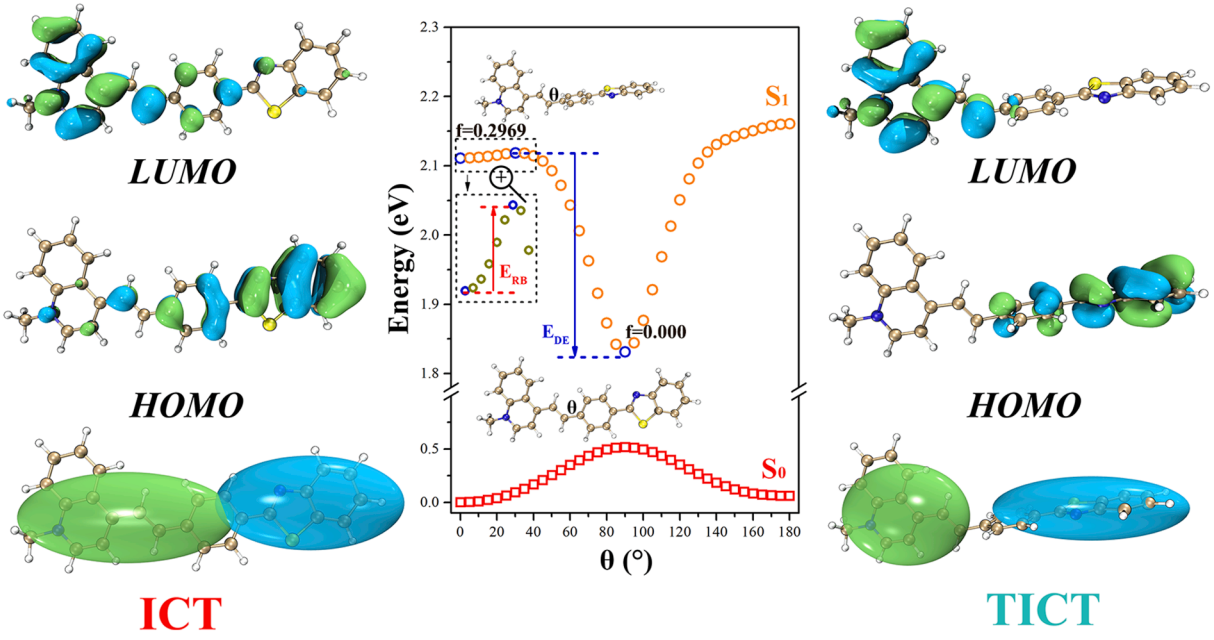

Fig. 3. Theoretical calculations and descriptions of HOMO/ LUMO energy levels in the molecule BQL. TDDFT calculations demonstrate energy changes in different states of the molecule as rotation angle (θ_1) increases. An isosurface map of the BQL hole is also displayed.

conjugate system was broken in the S_1 state, resulting in complete charge separation and the subsequent quenching of fluorescence emission.

According to previous research, the rotation barrier (E_{RB}) and the driving energy (E_{DE}) are key parameters for evaluating whether or not the molecule can spontaneously transit from the ICT state to the TICT state [33]. We calculated the energy distribution of S_0 (BQL nearly planar) and S_1 (BQL contorted along a dihedral angle θ). According to Fig. 3, the E_{RB} of BQL was 0.0074 eV, and its E_{DE} was −1.82 eV. Hence, the TICT state occurred spontaneously, and in turn caused fluorescence quenching of BQL. While calculations revealed that the molecule could rotate spontaneously in low viscosity medium, molecule rotation was limited in high viscosity medium, resulting in enhanced fluorescence intensity. The above theory effectively explains the fluorescence phenomenon demonstrated in 3.1.

3.4. Cytotoxicity and co-localization assay

First, we performed an MTT assay to evaluate cytotoxicity at various BQL concentrations. Cytotoxicity was measured as the ratio of the ultraviolet absorption intensity at 490 nm in cells treated with BQL (at different concentrations) to the ultraviolet absorption intensity at 490 nm in untreated cells. As shown in Figure S6, the viability of cells treated with 100 μM BQL for 24 h remained above 82 %. The results show that BQL at low concentrations is non-cytotoxic although after incubation for a long time; therefore, it is safe for biological imaging.

In recent years, several organelle-targeting fluorescent chemosensors have been developed to monitor specific substances in organelles or the organelle microenvironment[34,35]. In the present study, A549 cells were first incubated with BQL and MitoTracker Green. As shown in Figure S7, the red channel reporting BQL fluorescence largely overlapped with the green channel marking mitochondria (Pearson's correlation coefficient, 0.95). Thus, the quinoline derivative cation structure of the chemosensor fulfills its design. To investigate off-target co-localization of BQL with other organelles, we performed a co-localization experiment using BQL and a lysosome-specific dye. As shown in Figure S8, BQL did not specifically target the lysosome (Pearson's correlation coefficient, 0.27). Together, these results demonstrate the mitochondrial specificity of the BQL chemosensor. Moreover, the results provide evidence that the BQL chemosensor can be used to specifically report on the mitochondrial biological microenvironment.

At the same time, we verified the effect of the concentration of BQL on the fluorescence intensity of A549 cells. 8 μM, 10 μM and 12 μM of BQL were added into A549 cells to observe the fluorescence intensity. The results showed that there was no significant difference, indicating that the concentration of the probe had almost no obvious effect on the fluorescence intensity, and the variation of fluorescence intensity was caused by the changes of microviscosity (Figure S9).

3.5. Detection of mitochondrial viscosity

To investigate the BQL response to natural variations in intracellular viscosity, we manipulated the viscous microenvironment in A549 cells. According to previous reports, monensin, nystatin, and autophagy induction can all affect mitochondrial viscosity[22,36]. In our cell-based experiments, we manipulated mitochondrial viscosity states using the above three methods, and then added BQL to facilitate measurements of viscosity by confocal imaging.

Monensin is an antibiotic commonly used as a growth promoter in animals. The toxicological mechanism of monensin requires the formation of a lipophile complex with Na^+ (or other cations), and this complex is able to pass freely into and out of the cell through the membrane. When the lipophile complex enters the cell, intracellular Ca^{2+} levels increase, resulting in an imbalance in intracellular ions, and a consequent enhancement of viscosity[37,38]. Because monensin principally targets organs that require a lot of energy production (e.g., hearts and kidneys), mitochondria are inferred to be the major suborganelle to which monensin locates. Nystatin is an antibiotic with a conjugated polyene macrolide structure. Like monensin, nystatin is an ionic carrier with high membrane permeability. Nystatin is proposed to both enhance mitochondrial viscosity and to increase the diffusion of intracellular material out of the cell[38,39]. Both these activities are likely to lead to abnormal changes in nystatin-treated cells.

To manipulate the mitochondrial viscous microenvironment, A549 cells were treated with nystatin or monensin for a relatively short incubation period (to minimize any adverse biological reactions induced by these ionic carriers). The pre-treated A549 cells were then incubated

with BQL. Finally, the cells were washed three times with PBS, and then imaged using confocal microscopy. As shown in Fig. 4A1 and Fig. 4B1, untreated cells (containing only BQL) demonstrated enhanced brightness (compared with control cells). Thus, BQL demonstrates spontaneous fluorescence in the normal microenvironment. However, the confocal fluorescence intensity was markedly enhanced after monensin or nystatin treatment for 25 min (Fig. 4B1, 4C1, and 4D1). As shown in Fig. 4E, the degree of mitochondrial viscosity enhancement induced by monensin was slightly higher than that induced by nystatin. These results are consistent with those of previous studies. Together, the above experiments provide evidence that BQL is a powerful tool for detecting variations in mitochondrial viscosity.

3.6. Mitochondrial autophagy induced viscosity change

Mitochondrial autophagy is an important cellular stress response. In the event of cell stress, the mitochondrial internal environment can become compromised, potentially leading to dysfunction. The main function of mitochondrial autophagy is to remove these abnormal mitochondria, and to maintain a stable cell environment to ensure normal energy metabolism. This self-regulation mechanism relies on lysosomal decomposition and the recycling of damaged mitochondria to regenerate the nutrients needed for normal cell activities. Mitochondrial autophagy induced by starvation is a specific type of selective autophagy. In the event of mitochondrial nutrient deficiency, autophagosomes selectively bind to damaged mitochondria and then fuse with lysosomes to facilitate degradation and recycling[40,41]. During the above process, mitochondrial viscosity inevitably changes.

In our experiments, we utilized serum-free medium for starvation induction and subsequent mitochondrial autophagy[42]. After starvation induction, the cells were incubated with BQL for 25 min and 60 min. BQL specific fluorescence in untreated A549 cells is demonstrated in Figure 5B1 (in comparison with control cells in Figure 5A1). When A549 cells treated with serum-free medium were incubated with BQL for 25 min, the fluorescence in the red channel was enhanced, which is consistent with an increase in mitochondrial viscosity (Figure 5B1 and 5C1). When A549 cells treated with serum-free medium were incubated with BQL for 60 min, the morphology of A549 cells was significantly changed, which is consistent with the proposal that mitophagy had occurred during this period (Figure 5D1). Furthermore, BQL fluorescence intensity at 60 min was further enhanced (compared with 25 min incubation), indicating that mitochondrial viscosity was increasing in real-time during the process of mitophagy (Figure 5C1 and 5D1). Thus, changes in mitochondrial viscosity are a natural phenomenon of biological systems. These results provide evidence that BQL can be used as a chemosensor to detect real-time viscosity changes during mitochondrial autophagy. Moreover, BQL was shown to be a superior tool for applications in microbiological systems.

3.7. Rapamycin induced viscosity change

Rapamycin is a novel macrolide immunosuppressive agent, which could play an essential role in the process of cell apoptosis and has been used as a commercial ion inducer. In our experiment, rapamycin was added to A549 cells and the cells were incubated for 15 min and 30 min. Image J was used to measure the fluorescence intensity, and the results showed that the fluorescence intensity gradually increased with the increase of induction time of rapamycin (Fig. 6), indicating the increase of mitochondrial viscosity during this process. It is further confirmed that BQL is an effective tool for monitoring intracellular viscosity changes.

4. Conclusions

In summary, we report the synthesis of a water-soluble mitochondrial viscosity chemosensor that uses a benzothiazole-quinoline group as a fluorophore. Moreover, we demonstrate that our novel BQL chemosensor has exceptional properties that favor its use as a mitochondrial viscosity chemosensor. BQL fluorescence intensity at its emission peak (560 nm) increased with solvent viscosity, showing a 14.3-fold increase

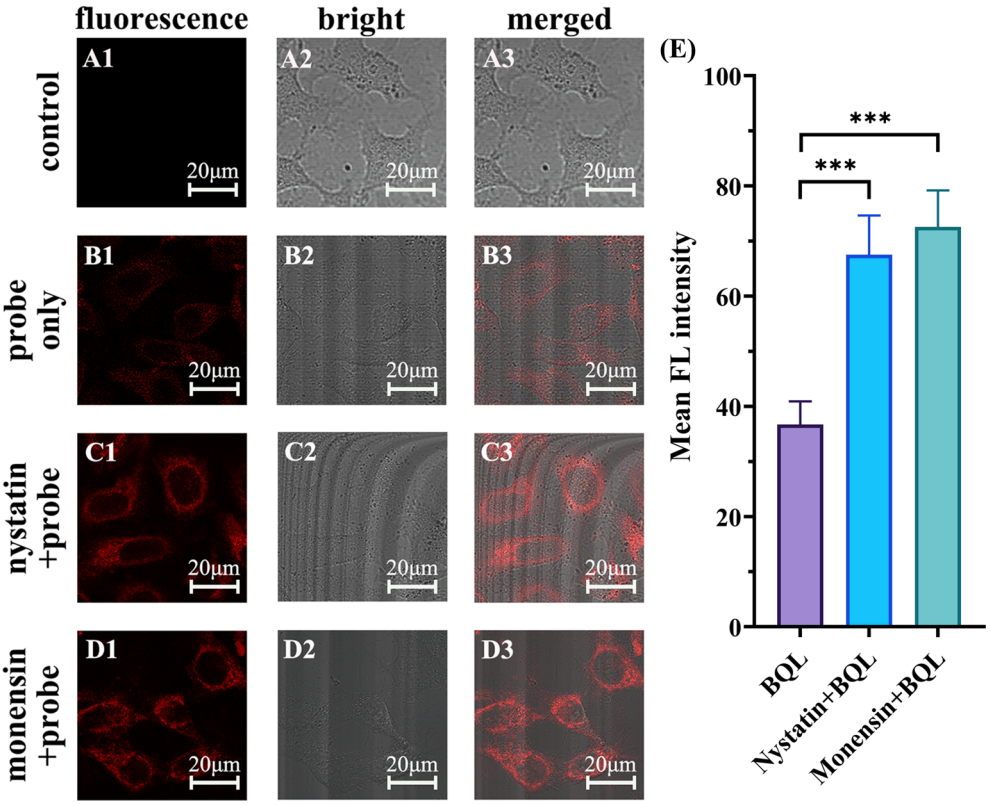

Fig. 4. (A1–A3) Confocal fluorescence images of control A549 cells. (B1–B3) Confocal fluorescence images of A549 cells after incubation with 10 μM BQL. (C1–C3) Confocal fluorescence images of A549 cells after incubation with nystatin for 25 min, followed by BQL for 20 min. (D1–D3) Confocal fluorescence images of A549 cells after incubation with monensin for 25 min, followed by BQL for 20 min. (E) Comparison of fluorescence intensities in (B1), (C1), and (D1). ***P < 0.001, data analyses were performed with an independent sample test with equal variances, means ± SD, n = 3. λ_{ex} = 405 nm, λ_{em} = 410–585 nm.

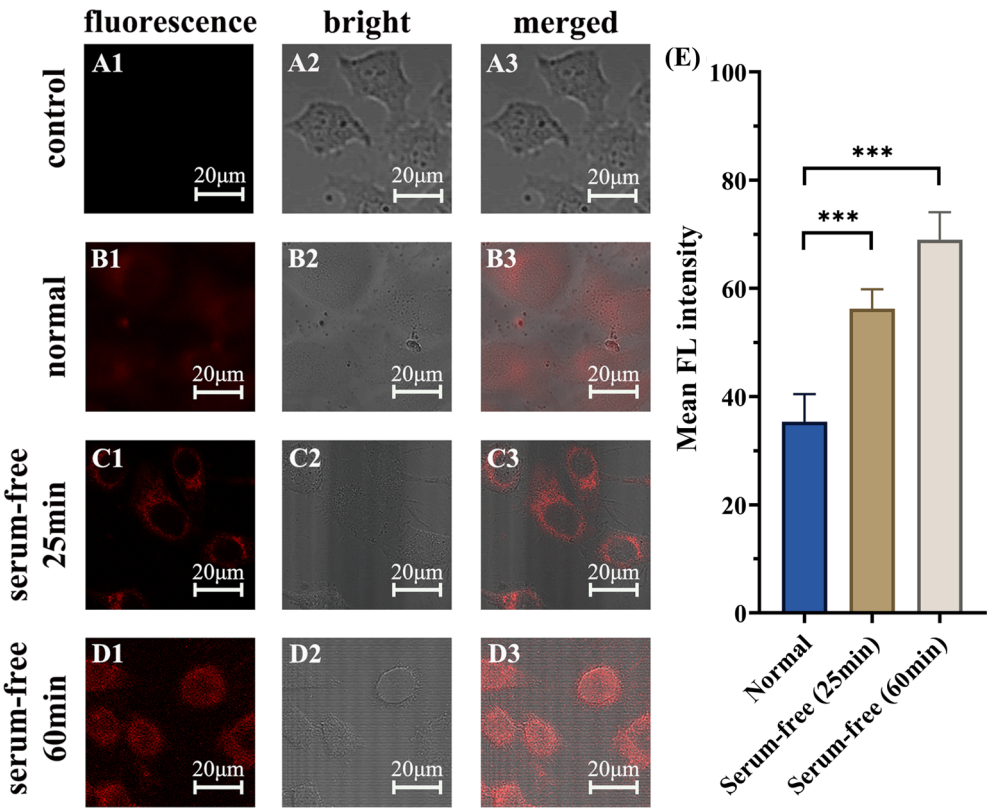

Fig. 5. (A1–A3) Confocal fluorescence images of control A549 cells. (B1–B3) Confocal fluorescence images of A549 cells after incubation with 10 μM BQL in normal medium for 25 min. (C1–C3) Confocal fluorescence images of A549 cells after incubation with 10 μM BQL in serum-free medium for 25 min. (D1–D3) Confocal fluorescence images of A549 cells after incubation with 10 μM BQL in serum-free medium for 60 min. (E) Comparison of fluorescence intensities in (B1), (C1), and (D1). ***P <0.001, data analyses were performed with an independent sample test with equal variances, means ± SD, n = 3. λ_{ex} = 405 nm, λ_{em}=410-585 nm.

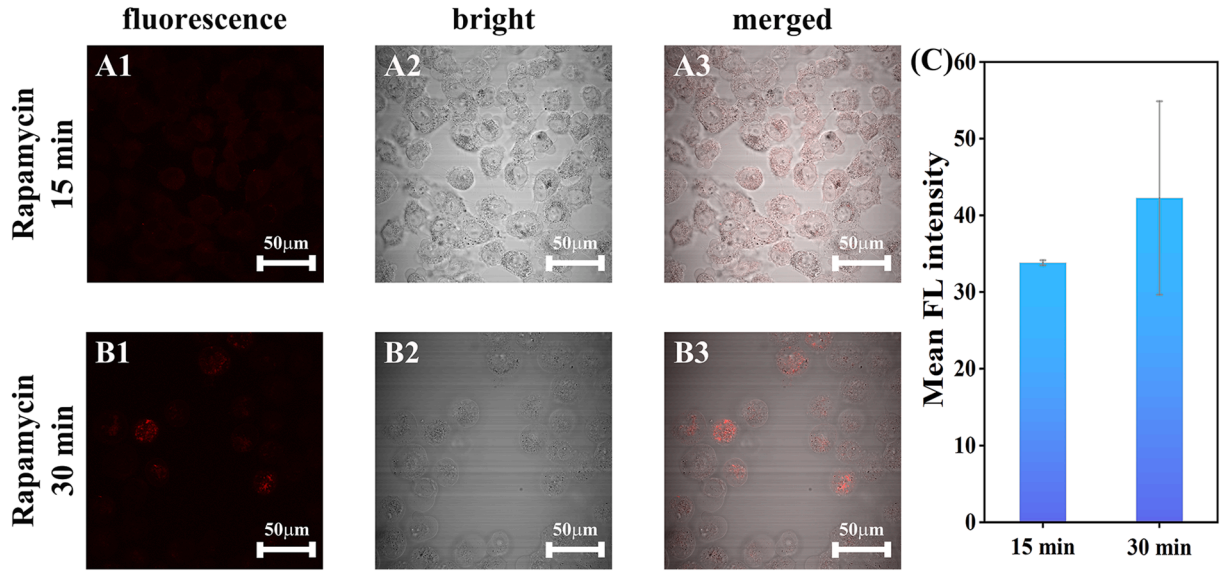

Fig. 6. (A1–A3) Confocal fluorescence images of A549 cells after incubation with rapamycin for 15 min, followed by BQL for 20 min. (B1–B3) Confocal fluorescence images of A549 cells after incubation with rapamycin for 30 min, followed by BQL for 20 min. (C) Comparison of fluorescence intensities in (A1) and (B1). λ_{ex} = 405 nm, λ_{em} = 410–585 nm.

from 0 % glycerol to 95 % glycerol. In biological studies, interference from auto-fluorescence is minimized because of the large Stokes shift (128 nm). Importantly, BQL can target mitochondria and distinguish changes in viscosity associated with various mitochondrial processes, including mitophagy. In future studies, our BQL chemosensor may be employed as a powerful tool for anticipating mitochondrial viscosity-related diseases.

CRediT authorship contribution statement

Siqi Zhang: Conceptualization, Investigation, Data curation, Validation, Writing – original draft. **Hong Zhang:** Data curation, Formal analysis, Investigation, Validation. **Lihe Zhao:** Writing – review & editing, Formal analysis. **Lanlan Xu:** Data curation, Formal analysis, Investigation. **Pinyi Ma:** Conceptualization, Project administration, Data curation, Writing – review & editing, Software. **Ping Ren:** . **Daqian Song:** Project administration, Funding acquisition, Resources,

Supervision.

Declaration of Competing Interest

The authors declare that they have no known competing financial interests or personal relationships that could have appeared to influence the work reported in this paper.

Acknowledgements

This work was supported by the National Natural Science Foundation of China (Grant Nos. 22074046 and 22004052).

Appendix A. Supplementary data

Supplementary data to this article can be found online at https://doi.org/10.1016/j.saa.2022.121799.

References

[1] M.K. Kuimova, S.W. Botchway, A.W. Parker, M. Balaz, H.A. Collins, H.L. Anderson, K. Suhling, P.R. Ogilby, Imaging intracellular viscosity of a single cell during photoinduced cell death, Nat. Chem. 1 (2009) 69–73.
[2] K. Luby-Phelps, The physical chemistry of cytoplasm and its influence on cell function: an update, Molecular Biology of the Cell 24 (2013) 2593–2596.
[3] K. Luby-Phelps, Physical properties of cytoplasm, Current opinion in cell biology 6 (1994) 3–9.
[4] O. Nadiv, M. Shinitzky, H. Manu, D. Hecht, C.T. Roberts Jr., D. LeRoith, Y. Zick, Elevated protein tyrosine phosphatase activity and increased membrane viscosity are associated with impaired activation of the insulin receptor kinase in old rats, The Biochemical Journal 298 (Pt 2) (1994) 443–450.
[5] G. Deliconstantinos, V. Villiotou, J.C. Stavrides, Modulation of particulate nitric oxide synthase activity and peroxynitrite synthesis in cholesterol enriched endothelial cell membranes, Biochemical pharmacology 49 (1995) 1589–1600.
[6] M. Fu, W. Shen, Y. Chen, W. Yi, C. Cai, L. Zhu, Q. Zhu, A highly sensitive red-emitting probe for the detection of viscosity changes in living cells, zebrafish, and human blood samples, Journal of Materials Chemistry B 8 (2020) 1310–1315.
[7] W.V. Humphreys, A. Walker, D. Charlesworth, Altered viscosity and yield stress in patients with abdominal malignancy: relationship to deep vein thrombosis, The British journal of surgery 63 (1976) 559–561.
[8] G.S. Zubenko, U. Kopp, T. Seto, L.L. Firestone, Platelet membrane fluidity individuals at risk for Alzheimer's disease: a comparison of results from fluorescence spectroscopy and electron spin resonance spectroscopy, Psychopharmacology 145 (1999) 175–180.
[9] A.M. Aleardi, G. Benard, O. Augereau, M. Malgat, J.C. Talbot, J.P. Mazat, T. Letellier, J. Dachary-Prigent, G.C. Solaini, R. Rossignol, Gradual alteration of mitochondrial structure and function by beta-amyloids: Importance of membrane viscosity changes, energy deprivation, reactive oxygen species production, and cytochrome c release, Journal of Bioenergetics and Biomembranes 37 (2005) 207–225.
[10] L. Wang, Y. Xiao, W. Tian, L. Deng, Activatable Rotor for Quantifying Lysosomal Viscosity in Living Cells, Journal of the American Chemical Society 135 (2013) 2903–2906.
[11] C. Ma, W. Sun, L. Xu, Y. Qian, J. Dai, G. Zhong, Y. Hou, J. Liu, B. Shen, A minireview of viscosity-sensitive fluorescent probes: design and biological applications, Journal of Materials Chemistry B 8 (2020) 9642–9651.
[12] M. Fu, Y. Sun, M. Kenry, H. Zhang, W. Zhou, Y. Shen, Q.Z.u. Hu, A dual-rotator fluorescent probe for analyzing the viscosity of mitochondria and blood, Chemical Communications 57 (2021) 3508–3511.
[13] R. Guo, J. Yin, Y. Ma, G. Li, Q. Wang, W. Lin, A novel NIR probe for detection of viscosity in cellular lipid droplets, zebra fishes and living mice, Sensors and Actuators B-Chemical 271 (2018) 321–328.
[14] Y. He, J. Shin, W. Gong, P. Das, J. Qu, Z. Yang, W. Liu, C. Kang, J. Qu, J.S. Kim, Dual-functional fluorescent molecular rotor for endoplasmic reticulum microviscosity imaging during reticulophagy, Chemical Communications 55 (2019) 2453–2456.
[15] Y.-L.-P. Ow, D.R. Green, Z. Hao, T.W. Mak, Cytochrome c: functions beyond respiration, Nature Reviews Molecular Cell Biology 9 (2008) 532–542.
[16] S.A. Detmer, D.C. Chan, Functions and dysfunctions of mitochondrial dynamics, Nature Reviews Molecular Cell Biology 8 (2007) 870–879.
[17] D. Wang, J. Wang, G.M.C. Bonamy, S. Meeusen, R.G. Brusch, C. Turk, P. Yang, P. G. Schultz, A Small Molecule Promotes Mitochondrial Fusion in Mammalian Cells, Angewandte Chemie-International Edition 51 (2012) 9302–9305.
[18] H.M. McBride, M. Neuspiel, S. Wasiak, Mitochondria: More than just a powerhouse, Current Biology 16 (2006) R551–R560.
[19] R. Del Bo, M. Moggio, M. Rango, S. Bonato, M.G. D'Angelo, S. Ghezzi, G. Airoldi, M.T. Bassi, M. Guglieri, L. Napoli, C. Lamperti, S. Corti, A. Federico, N. Bresolin, G. P. Comi, Mutated mitofusin 2 presents with intrafamilial variability and brain mitochondrial dysfunction, Neurology 71 (2008) 1959–1966.
[20] S. Zuchner, P. De Jonghe, A. Jordanova, K.G. Claeys, V. Guergueltcheva, S. Cherninkova, S.R. Hamilton, G. Van Stavern, K.M. Krajewski, J. Stajich, I. Tournev, K. Verhoeven, C.T. Langerhorst, M. de Visser, F. Baas, T. Bird, V. Timmerman, M. Shy, J.M. Vance, Axonal neuropathy with optic atrophy is caused by mutations in mitofusin 2, Annals of Neurology 59 (2006) 276–281.
[21] G.J. Nie, A.D. Sheftel, S.F. Kim, P. Ponka, Overexpression of mitochondrial ferritin causes cytosolic iron depletion and changes cellular iron homeostasis, Blood 105 (2005) 2161–2167.
[22] Y. Zhang, Z. Li, W. Hu, Z. Liu, A Mitochondrial-Targeting Near-Infrared Fluorescent Probe for Visualizing and Monitoring Viscosity in Live Cells and Tissuese, Analytical Chemistry 91 (2019) 10302–10309.
[23] L. Zhu, M. Fu, B. Yin, L. Wang, Y. Chen, Q. Zhu, A red-emitting fluorescent probe for mitochondria-target microviscosity in living cells and blood viscosity detection in hyperglycemia mice, Dyes and Pigments 172 (2020) 107859.
[24] B. Chen, S. Mao, Y. Sun, L. Sun, N. Ding, C. Li, J. Zhou, A mitochondria-targeted near-infrared fluorescent probe for imaging viscosity in living cells and a diabetic mice model, Chemical Communications 57 (2021) 4376–4379.
[25] D. Wang, B.Z. Tang, Aggregation-Induced Emission Luminogens for Activity-Based Sensing, Accounts of Chemical Research 52 (2019) 2559–2570.
[26] J. Zhang, X. Chai, X.-P. He, H.-J. Kim, J. Yoon, H. Tian, Fluorogenic probes for disease-relevant enzymes, Chemical Society Reviews 48 (2019) 683–722.
[27] L. Wu, A.C. Sedgwick, X. Sun, S.D. Bull, X.-P. He, T.D. James, Reaction-Based Fluorescent Probes for the Detection and Imaging of Reactive Oxygen, Nitrogen, and Sulfur Species, Accounts of Chemical Research 52 (2019) 2582–2597.
[28] S. Sasaki, G.P.C. Drummen, G.-I. Konishi, Recent advances in twisted intramolecular charge transfer (TICT) fluorescence and related phenomena in materials chemistry, Journal of Materials Chemistry C 4 (2016) 2731–2743.
[29] A.S. Klymchenko, Solvatochromic and Fluorogenic Dyes as Environment-Sensitive Probes: Design and Biological Applications, Accounts of Chemical Research 50 (2017) 366–375.
[30] M.A. Haidekker, T.T. Ling, M. Anglo, H.Y. Stevens, J.A. Frangos, E.A. Theodorakis, New fluorescent probes for the measurement of cell membrane viscosity, Chemistry & Biology 8 (2001) 123–131.
[31] X. Song, H. Bian, C. Wang, M. Hu, N. Li, Y. Xiao, Development and applications of a near-infrared dye-benzylguanine conjugate to specifically label SNAP-tagged proteins, Organic & Biomolecular Chemistry 15 (2017) 8091–8101.
[32] A.L. Stadler, J.O. Delos Santos, E.S. Stensrud, A. Dembska, G.L. Silva, S. Liu, N. I. Shank, E. Kunttas-Tatli, C.J. Sobers, P.M.E. Gramlich, T. Care, L.A. Peteanu, B. M. McCartney, B.A. Armitage, Fluorescent DNA Nanotags Featuring Covalently Attached Intercalating Dyes: Synthesis, Antibody Conjugation, and Intracellular Imaging, Bioconjugate Chemistry 22 (2011) 1491–1502.
[33] C. Wang, Q. Qiao, W. Chi, J. Chen, W. Liu, D. Tan, S. McKechnie, D. Lyu, X.-F. Jiang, W. Zhou, N. Xu, Q. Zhang, Z. Xu, X. Liu, Quantitative Design of Bright Fluorophores and AIEgens by the Accurate Prediction of Twisted Intramolecular Charge Transfer (TICT), Angew Chem Int Edit 59 (2020) 10160–10172.
[34] T. Cao, L. Zhang, H. Ma, L. Zheng, Y. Cao, J. Wang, Y. Yang, J. Zhang, W. Qin, Y. Liu, Near-infrared ratio fluorescent sensor for the study of PGP-1 in inflammation and tumor mice, Sensors and Actuators B: Chemical 338 (2021) 129841.
[35] Y. Yang, Y. Hu, W. Shi, H. Ma, A near-infrared fluorescence probe for imaging of pantetheinase in cells and mice in vivo, Chem Sci 11 (2020) 12802–12806.
[36] Z. Zou, Q. Yan, S. Ai, P. Qi, H. Yang, Y. Zhang, Z. Qing, L. Zhang, F. Feng, R. Yang, Real-Time Visualizing Mitophagy-Specific Viscosity Dynamic by Mitochondria-Anchored Molecular Rotor, Analytical Chemistry 91 (2019) 8574–8581.
[37] A.C. Souza, F.S. Machado, M.R.N. Celes, G. Faria, L.B. Rocha, J.S. Silva, M.A. Rossi, Mitochondrial damage as an early event of monensin-induced cell injury in cultured fibroblasts L929, Journal of Veterinary Medicine Series a-Physiology Pathology, Clinical Medicine 52 (2005) 230–237.
[38] M. Tang, Z. Huang, X. Luo, M. Liu, L. Wang, Z. Qi, S. Huang, J. Zhong, J.-X. Chen, L. Li, D. Wu, L. Chen, Ferritinophagy activation and sideroflexin1-dependent mitochondria iron overload is involved in apelin-13-induced cardiomyocytes hypertrophy, Free Radical Biology and Medicine 134 (2019) 445–457.
[39] S.P. Soltoff, L.J. Mandel, Potassium transport in the rabbit renal proximal tubule: effects of barium, ouabain, valinomycin, and other ionophores, The Journal of membrane biology 94 (1986) 153–161.
[40] Y. Liu, J. Zhou, L. Wang, X. Hu, X. Liu, M. Liu, Z. Cao, D. Shangguan, W. Tan, A Cyanine Dye to Probe Mitophagy: Simultaneous Detection of Mitochondria and Autolysosomes in Live Cells, Journal of the American Chemical Society 138 (2016) 12368–12374.
[41] C.W. Wang, D.J. Klionsky, The molecular mechanism of autophagy, Molecular Medicine 9 (2003) 65–76.
[42] C. Sun, Z. Wang, L. Yue, Q. Huang, Q. Cheng, R. Wang, Supramolecular Induction of Mitochondrial Aggregation and Fusion, J Am Chem Soc 142 (2020) 16523–16527.